Electronic Supplementary Information

Polymer Brushes in Solid State Nanopores Form an Impenetrable Entropic Barrier for Proteins

Gustav Emilsson,[1] Kunli Xiong,[1] Yusuke Sakiyama,[2] Bita Malekian,[1] Viktor Ahlberg Gagnér,[1] Rafael L. Schoch,[2] Roderick Y. H. Lim[2] and Andreas B. Dahlin.[*1]*

[1] Department of Chemistry and Chemical Engineering Chalmers University of Technology, 41296 Göteborg, Sweden.

[2] Biozentrum and the Swiss Nanoscience Institute, University of Basel, 4056 Basel, Switzerland.

* Corresponding author: adahlin@chalmers.se

Materials and Methods

Nanofabrication: The different steps in the nanofabrication were generally performed as described in earlier work.[1-4] The colloids used were 158±4 nm polystyrene-sulphate (Microparticles, Germany). A maximum 1 nm Cr layer was deposited before Au to improve adhesion. The dry etching time and power for making nanowells was typically 50 W for 7 min ($CF_4 + O_2$), resulting in ~100 nm deep wells as measured by cross-section imaging, while the wet etching time for nanocaves was typically 40 s, resulting in ~100 nm deep caves. The wet etching step was done in buffered oxide etch (15%) and samples were thoroughly rinsed with distilled water afterwards. Prior to experiments all samples were cleaned with basic piranha for 25 min, which also removes any remaining Al_2O_3. After rinsing with milli-Q water the samples were sonicated in ethanol (99.7 %) for five minutes. The samples were then dried using nitrogen and immediately mounted in the flow-cell.

Chemicals: Phosphate buffered saline (PBS) tablets were dissolved in milli-Q water. Avidin (NeutrAvidin, ThermoFisher) and bovine serum albumin (Sigma) were stored frozen at 1 g/L in water while bovine adult sterile serum (Sigma) was kept refrigerated. Thiol terminated PEG was purchased from Nanocs (2 kg/mol), Rapp Polymere (10 kg/mol) and LaysanBio (20 kg/mol). Grafting-to was performed as described earlier.[5] We noted that the polymer binding rate to the nanostructures varied depending on the manufacturer. This can be attributed to a varying fraction of active thiol groups in the product. (Note that it is not possible to speed up the binding by increasing PEG concentration in the Na_2SO_4 solution as this leads to precipitation.)

Electron microscopy: Images were acquired using a Zeiss Supra 60 VP. Diameters and pore densities were determined by image analysis in MATLAB as in previous work.[4] The scale bar in the software was used to define distance per pixel. To reduce any noise in the images, while

preserving edges, a Gaussian bilateral filter and a Wiener filter were applied. The holes were then identified using a circle finding Hough transform.

AFM: Force-volume maps were recorded using a Bioscope catalyst AFM with gold coated OBL-10 cantilevers (Bruker, USA) with spring constant 0.006-0.009 N/m. Before use, the cantilevers were passivated using droplet incubation of 1 mM $C_{17}H_{36}O_4S$ (nanoScience Instruments, USA) in PBS for 10 min and rinsed with PBS. Each 500 × 500 nm^2 force volume map was recorded with 32 × 32 data points or 1024 force curves in PBS. The ramp size was 500 nm and the maximum (trigger) force applied was 500 pN. After each measurement additional force curves were obtained on a clean glass substrate in PBS as a control for tip contamination. Baseline corrected force–distance curves were fitted with a double exponential function. The brush heights were obtained by setting a force threshold of 1 pN for the fit to the experimental data. High speed AFM (RIBM, Japan) was generally performed as in previous work,[6] with a homebuilt scanner that achieved a maximum scan speed of 200 ms per frame. AC10 cantilevers (Olympus) were used for all measurements. The nominal spring constant was 0.1 N/m and the resonance frequency in liquid was ~400 kHz. Amorphous carbon tips were fabricated on top of the silicon lever 10° tilted from the direction perpendicular to the sample surface using a scanning electron microscope. The line profiles from high speed AFM data were extracted after correcting for drift in the surface plane by normalized cross correlation methods implemented in MATLAB and Python. In the first step, a reference frame and feature (e.g. pore edge) was selected from each movie and all the remaining frames were adjusted by translation in xy-plane. The optimal translation vector was obtained by maximization of a normalized cross correlation coefficient between the feature in the frame being translated and the feature in the reference frame.

SPR: The angular reflectivity spectrum was obtained using a SPR Navi instrument (BioNavis) with ordinary Au sensor slides. Fresnel fitting was done in MATLAB using transfer matrix formalism.[2]

Fluorescence: Fluorescence measurements were conducted using a Zeiss Axio Imager Z2 upright microscope equipped with a Axiocam506 camera. Transport was measured using a Plan-Apochromat 63× water immersion objective (NA = 1.0) and a 300 µL droplet of PBS buffer placed on top of the membrane. After the first frame was captured 0.8 µM fluorophore (BSA or biocytin labeled with Alexa 488, ThermoFisher) was injected in the flow chamber (chamber volume ~300 µL below the membrane) using a peristaltic pump (1.5 mL was injected in ~80 s). Images were acquired every 20 s with a 100 ms exposure time. The fluorescence was analyzed by defining a 25×25 μm^2 square starting 25 µm from the membrane edge. The initial frame (background) of each image stack was subtracted and then all values were normalized to the fluorescence in the center of the membrane after 10 minutes.

Additional nanostructure characterization

Fig. 1 shows a sample with the largest pores that could still be sealed by polymer brushes (no detectable plasmonic response from protein adsorption). The histogram shows that the highest diameters (except for an extremely small fraction of outliers) are exactly 100 nm. Examples of cross-section images are shown. See literature for more images.[3]

The established procedure of anisotropic etching through a supporting Si wafer was used to produce membranes with nanopores, with lateral dimensions defined by UV lithography. Fig. 2 shows an example of a membrane approximately 120×120 μm^2 in size. Since there are ~10 pores on average per μm^2 the total number of pores contributing to the transport in the fluorescence measurements (one membrane) is well above 10^5.

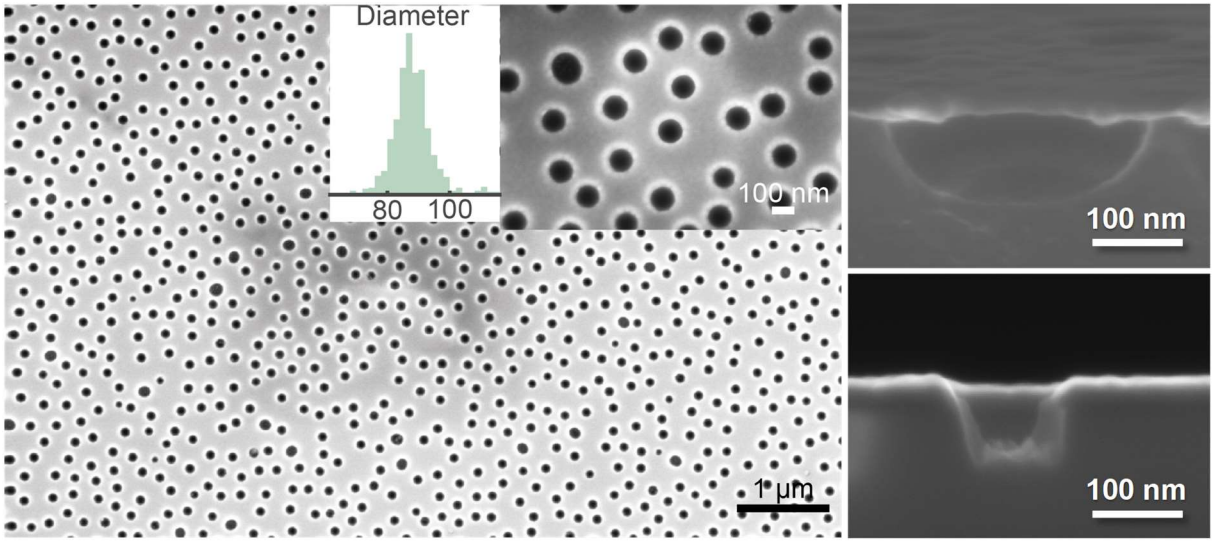

Figure 1. Images and diameter histogram for the largest nanopores (nanowells) that could be sealed by 20 kg/mol PEG. Also shown are examples of cross section images of a nanocave and a nanowell, where both are 100 nm in diameter and 100 nm deep.

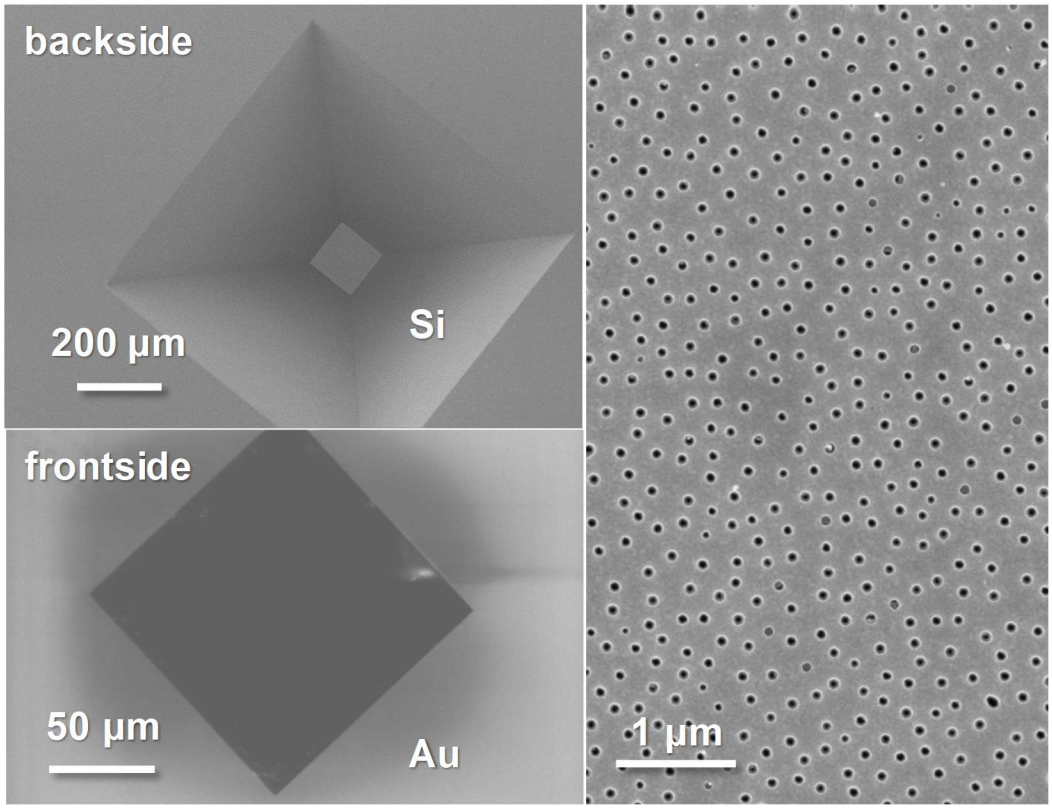

Figure 2. Example of pores in a membrane. The left images show the backside and frontside of a 50 nm Si_3N_4 membrane in a 500 µm thick Si wafer. Each membrane is approximately 120×120 μm^2. The right image shows the nanopores imaged from the frontside.

Quartz crystal microbalance (QCM) results

QCM with dissipation monitoring was used to verify the material-specific surface chemistry. Measurements were performed using quartz crystal microbalance with dissipation monitoring (Q-sense E4, Biolin Scientific). Two types of sensor crystals were used: Clean gold modified with 20 kg/mol PEG in the same manner as the nanocaves and sensor crystals coated with silica (Biolin Scientific). Fig. 3a shows the response upon addition of different proteins in PBS buffer. As expected, the PEG coated Au shows no detectable protein binding, neither for serum (10× dilution) or avidin. On silica there is considerable binding of avidin and even more for serum, in agreement with a dense protein monolayer. All binding was irreversible, i.e. the signal did not change when rinsing the chamber.

Fig. 3b shows the response from avidin when introduced in 0.9 M Na_2SO_4 to the same surfaces. First, a step-like response is observed when changing the bulk medium, but due to the strong dehydration of the brush[7] the response of the brush surface is actually inverted compared to clean silica. Further, some protein adsorption was detected on the brush as expected when it is not well hydrated, but all proteins were released again upon rinsing. Also, avidin adsorbed equally to silica in PBS as in 0.9 M Na_2SO_4. This confirms that the plasmonic response observed when adding avidin in theta solvent conditions is indeed due to open pores (see main text). The grafting of 20 kg/mol PEG to Au was also measured, which gave a saturated signal of ~250 Hz after ~6 h (not shown).

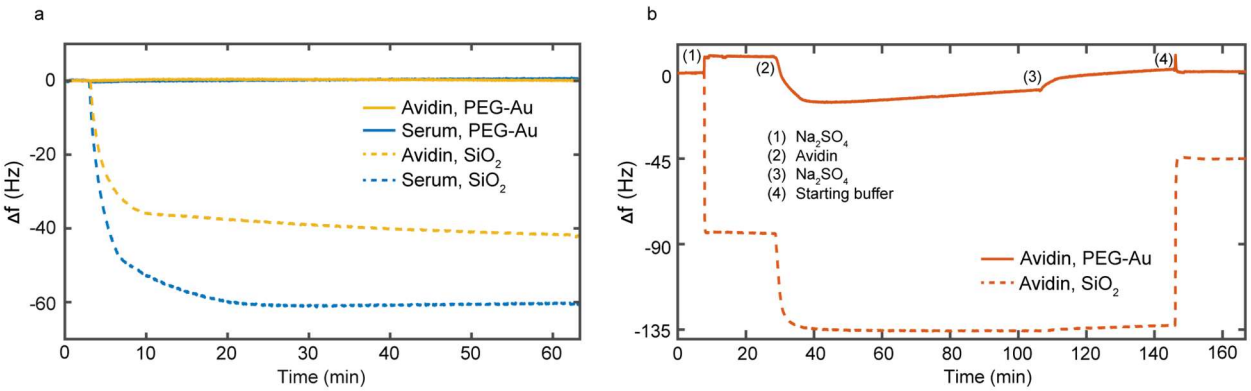

Figure 3. (a) QCM response upon addition of proteins to PEG-modified Au or SiO_2 in PBS. (b) QCM response upon switching to 0.9 M Na_2SO_4 and introducing avidin.

Measuring brush height by SPR

The dry brush thickness was determined from the angular SPR spectra in air (Fig. 4a) using a refractive index of 1.456 for PEG.[5] The grafting density was calculated from the known molecular weights and a density of 1.09 g/cm^3. The height of the hydrated brushes were determined by analyzing the full reflectivity spectrum, including the total internal reflection angle, upon changing the bulk refractive index with proteins. Previous work explains this "non-invasive probes" method.[7] In brief, a higher response means that the brush is thinner because it occupies less of the probing volume. Repeated injections of BSA (10 g/L) were performed over the formed brushes (Fig. 4b). It should be noted that this method relies on the assumption that the brush excludes proteins fully up to a certain height, at which the concentration becomes equal to the bulk value through a step-like profile.[8] In principle it cannot be known to what extent this holds true and gradual increases in protein concentration (with distance from the surface) also gives consistent solutions to the Fresnel reflectivity. The resulting height should be interpreted as the characteristic level at which the protein concentration is strongly reduced compared to the bulk.

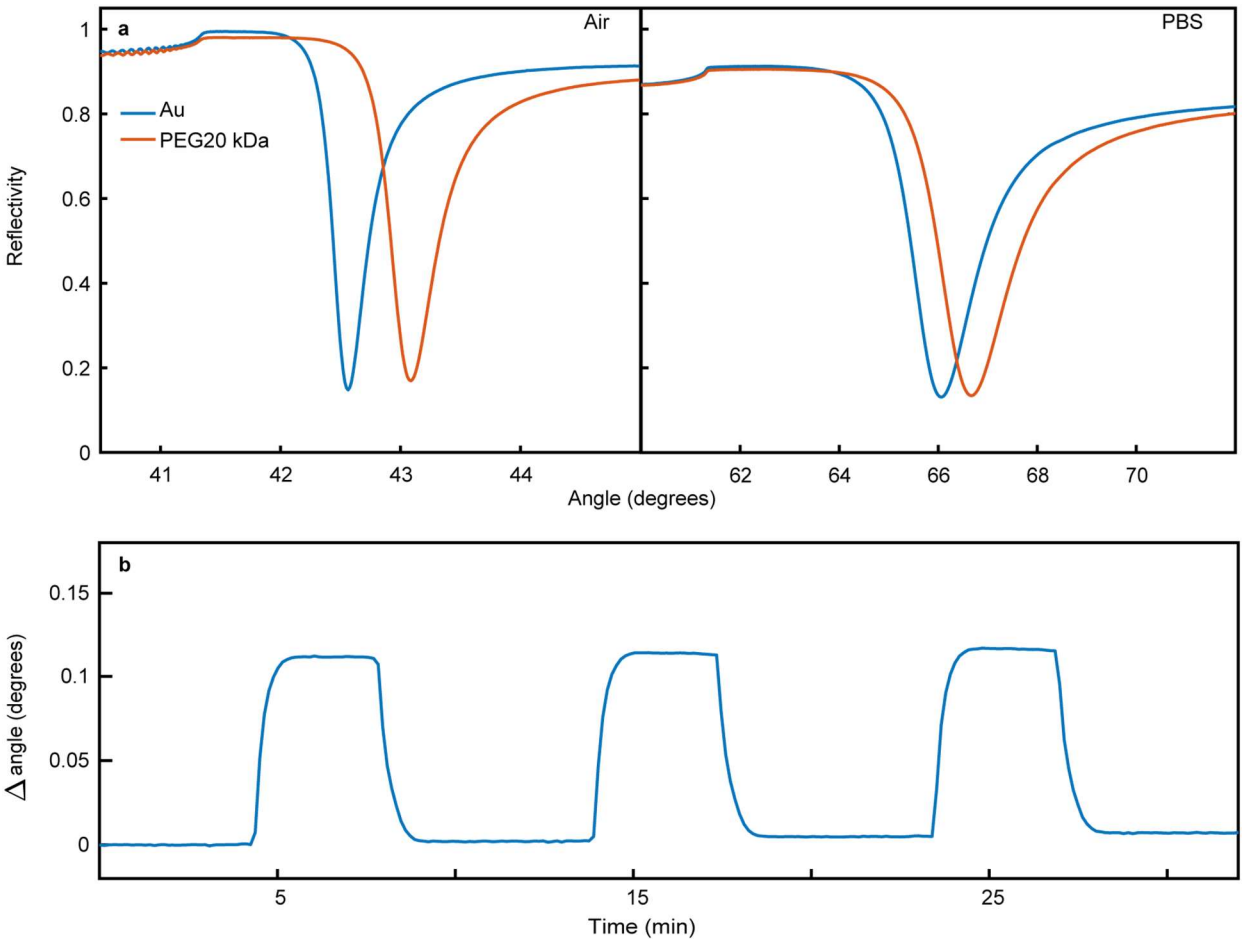

Figure 4. (a) Measured reflectivity spectra for gold surfaces before (blue) and after (red) binding of PEG 20 kg/mol in air and buffer. (b) Example of consecutive BSA injections used to probe the hydrated thickness of the PEG layer from the bulk response. The profiles were linearly related to the total internal reflection angle, confirming that adsorption did not contribute to the response.

High speed AFM

Three examples of high speed AFM videos are included in this publication, each showing a single nanocave modified with 2 kg/mol PEG or 20 kg/mol PEG as well as a bare cave.

Representative images of tips are shown in Fig. 5. The tip edge has a radius of curvature down to 5 nm, while the diameter increases to ~50 nm at a distance of about ~100 nm from the tip. Considering the tip shape together with the nanocave depth and diameter it is very reasonable that it can penetrate 70 nm apertures (unless blocked by PEG) but not reach all the way to the glass bottom of nanocaves (100 nm below Au).

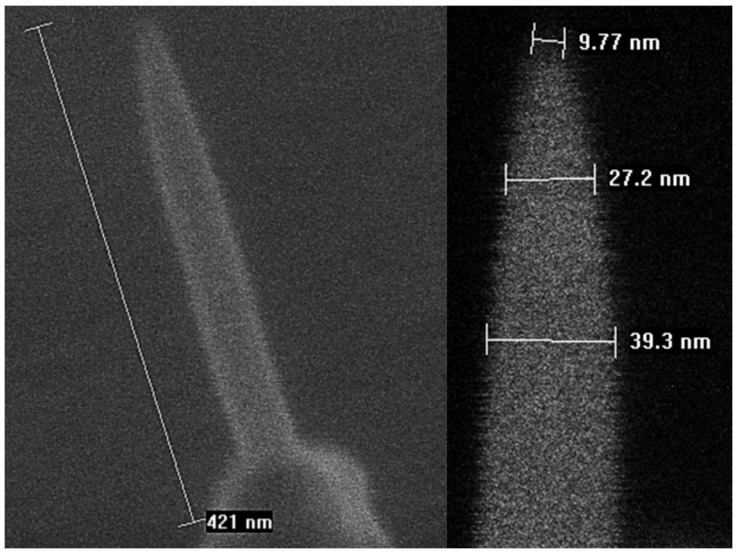

Figure 5. Examples of images of high speed AFM tips.

Theory of polymer brushes in pores

A basic model is presented here to account for how the concave surface inside a nanopore influences the polymer brush. The arguments follow the established theory of coils under good solvent conditions. The freely jointed chain model gives the conformational entropy (coil stretching) from the approximately Gaussian distribution of end-to-end distances. For a strongly-stretched brush we assume the free polymer end is on average located at a distance h from the surface, which defines the height of the brush in this (Alexander – de Gennes based) model. The conformational entropy is then:[9]

$$S = -\frac{3k_{\mathrm{B}}h^2}{2abN} + \text{constant} \qquad \text{(S1)}$$

Here a is the physical monomer length, b is the Kuhn length (defined as a step in the freely joined chain) and N is the degree of polymerization, such that the contour length is aN. Note that in the literature there is often a confusing mix up of a and b as well as N and the number of Kuhn steps. For more accurate models (not just power laws) it must be taken into account that the physical size of a monomer and chain flexibility are two different things.

The excluded volume entropy (self-avoidance) contribution is for low polymer volume fractions:

$$\Delta S = -\frac{k_{\mathrm{B}}vN^2}{V} \qquad \text{(S2)}$$

Here v is the excluded volume of one monomer and V is the total volume that one coil occupies (including solvent), so that for a brush with grafting density Γ (inverse of area per coil), $V = h/\Gamma$. The excluded volume contribution gives a term which is analogous to the contribution from the osmotic pressure of the solvent or a second virial expansion term. The solvent interactions are included in the sense that v varies with solvent quality.

The total free energy G of a coil in a planar brush can now be written as:

$$\frac{G}{k_B T} = \frac{\Gamma N^2 v}{h} + \frac{3h^2}{2abN} + \text{constant} \qquad \text{(S3)}$$

The free energy minimum occurs when the osmotic pressure balances the conformational entropy loss from stretching. Minimizing G with respect to h leads to the expression for the equilibrium brush height H:

$$H = \left[\frac{\Gamma abv}{3}\right]^{1/3} N \qquad \text{(S4)}$$

Simple expressions of this kind can accurately predict the brush height,[5] although it is not straightforward to find the most accurate values for a, b and v. Fortunately PEG in water is an extremely well-studied system. Here we argue for the most reasonable values of the parameters.

For the monomer size a the lowest suggested value is 0.28 nm, which represents the helical (gauche) configuration where a single water molecule forms hydrogen bonds to consecutive oxygens.[10] Experiments and theory have indicated that in the relaxed state >90% of the monomers maintain this configuration in water.[9] In the brush the coils are clearly stretched, but only up to ~30% of the contour length, which is well below the region where a majority of the monomers assume the trans state.[9] The trans state has a = 0.36 nm,[9] which agrees with an approximation based on tetrahedral (sp3 hybridization) atomic arrangement (assuming bond lengths of 1.54 Å for C-C and 1.43 Å for C-O). Based on the above we use the value a = 0.3 nm since we expect a minor part of the monomers to assume the trans state.

For the Kuhn length b there is relatively good consensus in the literature based on both calculations and experiments. We use b = 0.7 nm as determined from single molecule AFM experiments.[10] Similar studies have given values slightly below[9] (0.68 nm) or above[11] (0.76 nm).

For the excluded volume parameter v there is also variation in the literature, which to some extent can be attributed to the use of water with different ionic strength. Several reports are

experimentally studying the excluded volume (e.g. by osmometry) but v often becomes coupled to the monomer size a in the conformational entropy term by the approximation $v = a^3$.[12] Direct determinations of v are rarer. Here we use $v = 0.41^3 \approx 0.07$ nm^3 estimated by neutron reflectometry.[13] We acknowledge that there is clearly some uncertainty remaining in all the parameters a, b and v. However, as shown in the main text the model gives quite accurate results.

To account for the pore geometry we assume the coils are grafted to the interior walls of a cylindrical channel with radius R, so that the maximum extension is $h = R$ (Fig. 6).

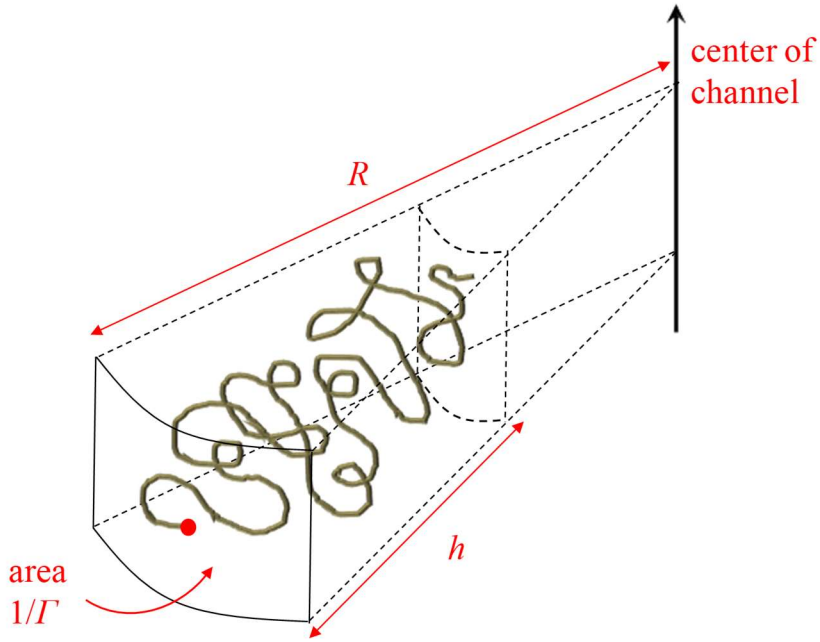

Figure 6. The volume occupied by a coil grafted to the wall of a cylindrical channel. It is assumed that the free end is just at the brush extension h from the wall towards the center.

If we consider a section of the channel with length Δz the total volume is $\pi R^2 \Delta z$ and the volume not occupied by the coils is $\pi[R - h]^2 \Delta z$. The total number of coils is $2\pi R \Gamma \Delta z$ and hence each coil now occupies a volume of:

$$V = \frac{\pi R^2 \Delta z - \pi\left[R - h\right]^2 \Delta z}{2\pi R \Delta z \Gamma} = \frac{2Rh - h^2}{2R\Gamma} \qquad \text{(S5)}$$

Note that if $R \rightarrow \infty$ the expression gives $V = h/\Gamma$, i.e. the result for a planar surface is recovered. We assume again that the free polymer terminal is at the height h for the conformational entropy and insert the new expression for the coil volume into the free energy sum to get the expression in the main text.

The equation cannot be solved for an explicit expression for H, but the expression can be easily evaluated numerically in order to find the minimum of G as a function of h for different values of R. As exemplified in Fig. 7, a minimum in G always occurs for some $H < R$, representing the brush extension in the cylindrical pore. The constant term from the conformational entropy will not depend on R and hence the free energy change imposed by the pore geometry can also be determined. Fig. 8 shows $G(h)$ plots for 20 kg/mol PEG at a grafting density of $\Gamma = 0.27$ nm^{-2}. The value of G and h at the minimum was determined numerically for several values of R to generate the plots in the main text.

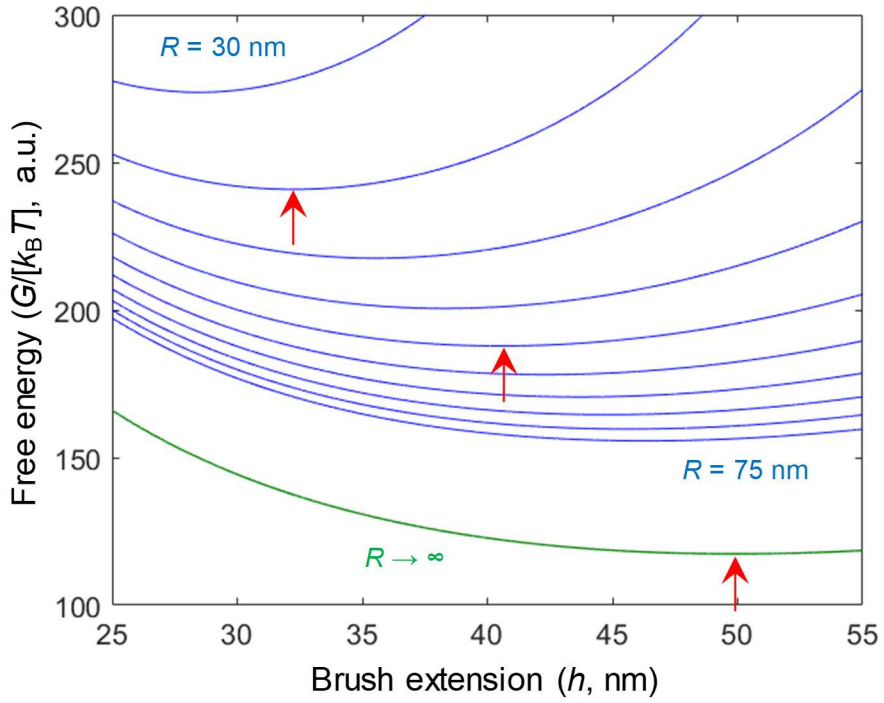

Figure 7. Example results of the model for the free energy per coil vs extension for the case of 20 kg/mol PEG at a grafting density of 0.27 nm^{-2}. The arrows indicate the minima predicted for a 100 nm pore, a 70 nm pore and a planar surface.

As discussed in the main text, the model shows two main effects due to the pore geometry: First, the extension of the coils decreases compared to a planar surface. Second, the free energy is considerably higher for a coil inside a pore (at the same grafting density) due to the high excluded volume entropy. It is also interesting to note that the energy minima in the plots are sharper for lower *R*.

Selective grafting to pore walls

To investigate if grafting of PEG 20 kg/mol to the pore walls would be sufficient to prevent protein translocation, 90 nm nanowells were incubated with PEG 20 kg/mol *before* removing the alumina layer protecting the top surface. Prior to incubation the samples were cleaned as follows: 5 minutes sonication in ethanol (99.7%), oxygen plasma for 30 minutes, ethanol rinsing and drying with nitrogen. The PEG grafting was performed as for other samples overnight. After rinsing with water and drying the samples using nitrogen, they were mounted in the liquid cell for the subsequent steps (Fig. S8). Removal of alumina only requires weakly basic conditions[2] (which is why a basic piranha cleaning could not be performed beforehand).

As a peripheral finding, these results indicate that there is no significant surface mobility of the grafted polymers. Further, sufficiently small thiolated molecules can potentially replace the 20 kg/mol on the surface,[5] but this is not the case for 10 kg/mol. Both these conclusions follow from the fact that the pores are sealed, which would not be the case if the 20 kg/mol coils had moved away from the pore region or been replaced by 10 kg/mol PEG. (As discussed in the main text the 10 kg/mol PEG can only seal apertures below 70 nm.)

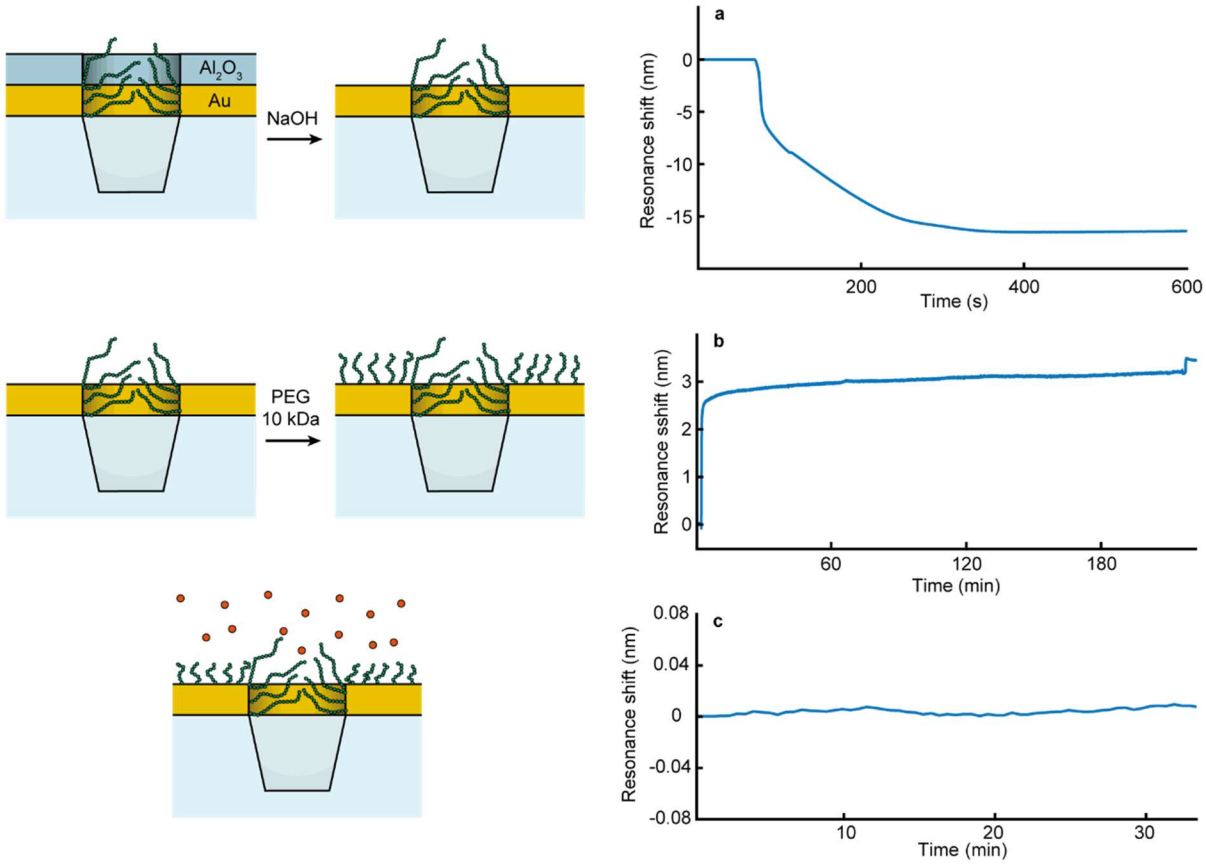

Figure 8. (a) Removal of the aluminum oxide layer using NaOH (10 mM), as indicated by the negative shift in resonance as Al_2O_3 ($n \approx 1.77$) is replaced with water ($n \approx 1.33$). (b) Binding of PEG 10 kg/mol to passivate the exposed planar gold. (c) Prevention of protein adsorption (see also main text).

References (also cited in main text)

1. A. B. Dahlin, M. Mapar, K. L. Xiong, F. Mazzotta, F. Hook and T. Sannomiya, *Adv. Opt. Mater.*, 2014, **2**, 556-564.

2. J. Junesch, T. Sannomiya and A. B. Dahlin, *ACS Nano*, 2012, **6**, 10405-10415.

3. B. Malekian, K. Xiong, G. Emilsson, J. Andersson, C. Fager, E. Olsson, E. M. Larsson-Langhammer and A. B. Dahlin, *Sensors*, 2017, **17**, 1444.

4. K. Xiong, G. Emilsson and A. B. Dahlin, *Analyst*, 2016, **141**, 3803-3810.

5. G. Emilsson, R. L. Schoch, L. Feuz, F. Hook, R. Y. H. Lim and A. B. Dahlin, *ACS Appl. Mater. Interf.*, 2015, **7**, 7505-7515.

6. Y. Sakiyama, A. Mazur, L. E. Kapinos and R. Y. H. Lim, *Nat. Nanotechnol.*, 2016, **11**, 719-723.

7. G. Emilsson, R. L. Schoch, P. Oertle, K. Xiong, R. Y. H. Lim and A. B. Dahlin, *Appl. Surf. Sci.*, 2017, **396**, 384-392.

8. R. L. Schoch, G. Emilsson, A. B. Dahlin and R. Y. H. Lim, *Polymer*, 2017, **132**, 362-367.

9. S. Liese, M. Gensler, S. Krysiak, R. Schwarzl, A. Achazi, B. Paulus, T. Hugel, J. P. Rabe and R. R. Netz, *ACS Nano*, 2016, **11**, 702-712.

10. F. Oesterhelt, M. Rief and H. E. Gaub, *New J. Phys.*, 1999, **1**, 6.

11. F. Kienberger, V. P. Pastushenko, G. Kada, H. J. Gruber, C. Riener, H. Schindler and P. Hinterdorfer, *Single Molecules*, 2000, **1**, 123-128.

12. P. L. Hansen, J. A. Cohen, R. Podgornik and V. A. Parsegian, *Biophys. J.*, 2003, **84**, 350-355.

13. E. Schneck, A. Schollier, A. Halperin, M. Moulin, M. Haertlein, M. Sferrazza and G. Fragneto, *Langmuir*, 2013, **29**, 14178-14187.